

A General Route Towards Defect and Pore Engineering in Graphene

Guibai Xie, Rong Yang, Peng Chen, Jing Zhang, Xuezeng Tian, Shuang Wu, Jing Zhao, Meng Cheng, Wei Yang, Duoming Wang, Congli He, Xuedong Bai, Dongxia Shi,* and Guangyu Zhang*

Defect engineering in graphene is important for tailoring graphene's properties thus applicable in various applications such as porous membranes and ultra-capacitors. In this paper, we report a general route towards defect- and pore- engineering in graphene through remote plasma treatments. Oxygen plasma irradiation was employed to create homogenous defects in graphene with controllable density from a few to $\approx 10^3$ (μm^{-2}). The created defects can be further enlarged into nanopores by hydrogen plasma anisotropic etching with well-defined pore size of a few nm or above. The achieved smallest nanopores are ≈ 2 nm in size, showing the potential for ultra-small graphene nanopores fabrication.

1. Introduction

Defects are of great importance in graphene. Through defect engineering, graphene's mechanical, electrical, chemical, and magnetic properties can be tailored.^[1–5] It has been reported that bandgap opening can be obtained in monolayer graphene by introducing proper amount of defects.^[6] Highly defected graphene can be used for ultra-capacitors with high performance.^[7–9] Graphene with nanopores can be used for DNA sequencing^[10–15] or molecular sieve^[16–21] through which only small molecules are allowed to pass. So far, different techniques including oxidation in ozone or in oxygen at elevated temperatures,^[22,23] focused electron-beam irradiation,^[19,24] scanning probe lithography,^[25] mask lithography^[26] and plasma irradiation^[27–34] have been developed to

introduce defects in graphene. However, creation of well-distributed defects or nanopores in graphene with controllable density and size remains a challenge.

In this paper, we report a general route towards defect- and pore- engineering in graphene through remote plasma treatments. Oxygen plasma irradiation, a violent process, was employed to create homogenous defects in graphene with controllable density through tuning the plasma conditions. The created defects were further enlarged into nanopores by mild hydrogen plasma anisotropic etching^[35–38] with well-defined pore size of a few nm or above. With this approach, we also successfully fabricated nanopores with the smallest size of ≈ 2 nm, which was comparable to that got via focused electron-beam irradiation previously.^[24]

2. Results and Discussion

2.1. Defects Creation by Oxygen-Plasma Irradiation

In this study, graphene samples were prepared by mechanical cleavage of highly oriented pyrolytic graphite (HOPG from SPI, Grade ZYA) and transferred onto 300-nm-thick SiO₂ substrates on which graphene can be identified under an optical microscope. Oxygen-plasma irradiation of graphene samples was carried out in a remote RF plasma system

G. B. Xie, R. Yang, P. Chen, J. Zhang, X. Z. Tian,
W. Shuang, J. Zhao, M. Cheng, W. Yang, D. M. Wang,
C. L. He, Prof. X. D. Bai, Prof. D. X. Shi, Prof. G. Y. Zhang

Beijing National Laboratory for

Condensed Matter Physics
and Institute of Physics

Chinese Academy of Sciences

Beijing 100190, China

E-mail: dxshi@aphy.iphy.ac.cn; gyzhang@aphy.iphy.ac.cn

DOI: 10.1002/smll.201303671



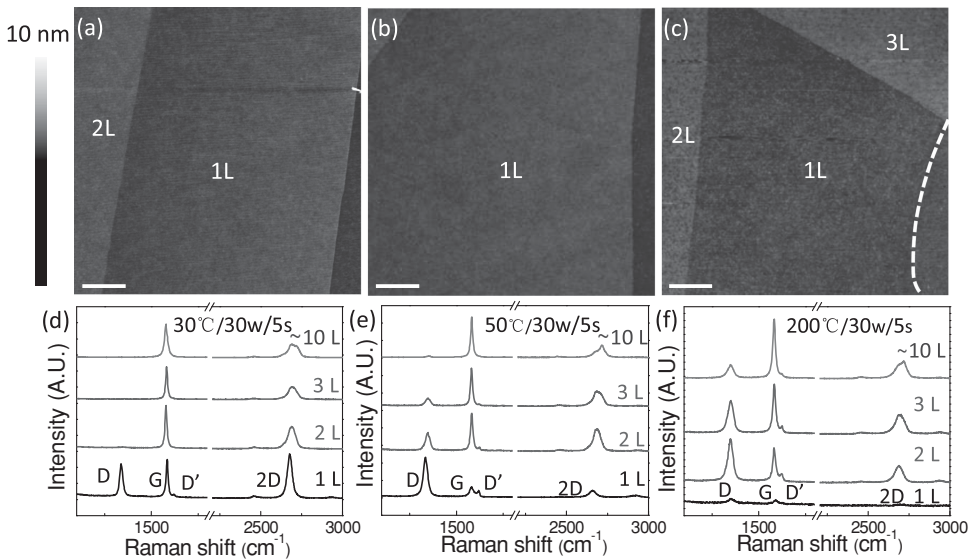


Figure 1. Defect creation in graphene by oxygen-plasma irradiation. (a)-(c) AFM images and (d)-(f) Raman spectra of three samples after oxygen-plasma irradiation at 30, 50, and 200 °C. Oxygen-plasma irradiation was carried out for graphene at $P = 30$ W and $t = 5$ s. The irradiated graphene shows no obvious changes as compared to the pristine samples at 30 and 50 °C in (a) and (b). However, the irradiation led to the removal of the monolayer graphene and serious damage of bilayer, trilayer, and multilayer graphene at 200 °C. Scale bar: 500 nm; color scale bar: 10 nm.

described elsewhere.^[34,35] Only pure oxygen was flowed for plasma generation under a fixed pressure of 0.6 Torr; and RF power (P), irradiation time (t) and sample temperature (T) were controlled to change the defect density.

We firstly carried out oxygen-plasma irradiation for graphene at $P = 30$ W and $t = 5$ s. **Figure 1a–c** show typical atomic force microscopy (AFM) images of graphene samples after irradiation at $T = 30$, 50, and 200 °C, respectively; and corresponding Raman spectra are shown in Figure 1d–f. From the AFM images shown in Figure 1a–b and S1 in the Supporting Information, we can see that the irradiated graphene shows no obvious changes as compared to the pristine samples. We guess these defects are mainly point defects since the plasma irradiation time is very short (5 s). However, Raman spectra of these samples after irradiation clearly show strong D peaks, which are characteristic features reflecting the defects existence in graphene.^[39] For each set of samples irradiated at 30 and 50 °C, monolayer graphene always shows much stronger Raman D peak than bilayer, trilayer or multilayer graphene, indicating that monolayer graphene is much more reactive. For graphene with same layer thickness, oxygen-plasma irradiation at increased temperature also introduces more defects, as evidenced from Figure 1d–f. As a result, oxygen-plasma irradiation at 200 °C led to the removal of the monolayer graphene and serious damage of bilayer, trilayer, and multilayer graphene (Figure 1c and 1f). Thereafter, we chose $T = 30$ and 50 °C oxygen-plasma irradiation in the following experiments.

We also carried out oxygen-plasma irradiation at $T = 30$ °C/ $P = 30$ W, $T = 30$ °C/ $P = 50$ W, and $T = 50$ °C/ $P = 30$ W for monolayer graphene for different

time durations. The corresponding Raman D/G peak intensity ratios ($I(D)/I(G)$) of these samples are shown **Figure 2a**. We can fit these experimental data into black, red, and blue lines in Figure 2a. The time evolution of $I(D)/I(G)$ as a function of t can be divided into two segments: $I(D)/I(G) \propto t$ before $I(D)/I(G)$ reaching a maximum (low-defect-density segment) and $I(D)/I(G) \propto t^{-1/2}$ after $I(D)/I(G)$ reaching the maximum (high-defect-density segment) according to previous studies.^[29] It has been shown that $I(D)/I(G)$ can be described as $\frac{I(D)}{I(G)} = \frac{C(\lambda)}{L_a^2}$ in the low-defect-density segment;^[40] and $\frac{I(D)}{I(G)} = C'(\lambda) \times L_a^2$ in the high-defect-density segment.^[41,42] Where L_a is the average interdefect distance, and $C(532 \text{ nm}) \approx 100$ and $C'(532 \text{ nm}) \approx 0.164$ is derived from ref [39]. Thus we can estimate the L_a for these samples shown in Figure 2a. For example, the $I(D)/I(G) = 0.12$ at $T = 30$ °C/ $P = 30$ W/ $t = 1$ s gives $L_a \approx 29$ nm, which is equivalent to a defect density of $\approx 1.2 \times 10^3 \mu\text{m}^{-2}$; and the $I(D)/I(G) = 4.1$ at $T = 30$ °C/ $P = 30$ W/ $t = 30$ s gives $L_a \approx 5$ nm, which is equivalent

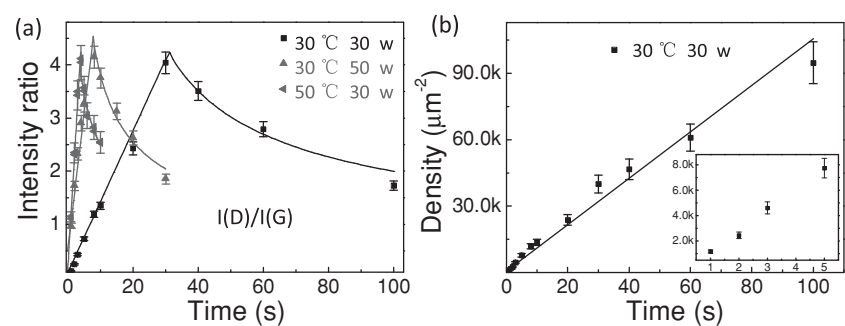


Figure 2. Estimation of defect density from Raman $I(D)/I(G)$. (a) Time evolution of $I(D)/I(G)$ for monolayer graphene treated by different oxygen-plasma irradiations. The solid lines (black, red, and blue) are line fits. $I(D)/I(G)$ can be described as $\frac{I(D)}{I(G)} = \frac{C(\lambda)}{L_a^2}$ in the low-defect-density segment; and $\frac{I(D)}{I(G)} = C'(\lambda) \times L_a^2$ in the high-defect-density segment. (b) Estimated defect density as a function of time derived from (a). A linear relationship was found between the defect density and t . The insert showed the defect density for $t = 1, 2, 3, 5$ s.

to a defect density of $\approx 4 \times 10^4 \mu\text{m}^{-2}$. In Figure 2b, we plotted the defect density as a function of t for the sample irradiated at $T = 30^\circ\text{C}/P = 30 \text{ W}$ and a linear relationship was found, just as expected. This linear relationship suggests that we can control the defect density in graphene by the irradiation time t at a fixed plasma power P and irradiation temperature T . The insert shows the defect density of $t = 1, 2, 3, 5 \text{ s}$. Besides, the peak or maximum positions shown in Figure 2a also reflect the defect creation ability related to the irradiation T and P . The down-shifted conditions are stronger at the same t .

2.2. Enlargement of the Created Defects into Nanopores

In order to enlarge these as-created defects into nanopores, we performed further hydrogen-plasma anisotropic etching, which reacts with graphene at the defect sites but wouldn't damage its perfect lattice.^[35,38] Hydrogen-plasma etching was carried out at $T = 400^\circ\text{C}, P = 15 \text{ W}$, and a gas pressure of 0.4 Torr. Under this etching condition, the lateral etching speed is $\approx 12 \text{ nm/min}$ for monolayer graphene and $\approx 4 \text{ nm/min}$ for bilayer graphene. **Figure 3a** shows the AFM images of

a monolayer graphene after oxygen-plasma irradiation at $T = 30^\circ\text{C}/P = 30 \text{ W}$ with $t < 1 \text{ s}$. After 1-min and 4-mins hydrogen-plasma etching, nanopores with sizes of $\approx 12 \text{ nm}$ (Figure 3b) and $\approx 50 \text{ nm}$ (Figure 3c), respectively, can be seen. For the bilayer sample (Figure 3d), the oxygen-plasma irradiation was carried out at $T = 30^\circ\text{C}/P = 50 \text{ W}/t = 60 \text{ s}$. After 10-mins and 25-mins hydrogen-plasma etching, the size of the pores is $\approx 40 \text{ nm}$ (Figure 3e) and $\approx 100 \text{ nm}$ (Figure 3f), respectively. Through this enlargement of defects by hydrogen-plasma etching, various nanopore sizes can thus be achieved by tuning the etching time durations. A size distribution of 100-nanopore in Figure 3c and 3f was shown in Figure 3g and 3h, respectively. The homogenous distribution showed the great reliability of the approach.

As shown above, the density of defects in graphene can be controlled by initial oxygen-plasma irradiation. Hydrogen-plasma etching can enlarge these created defects into visible nanopores thus allows direct counting of the number of defects. **Figure 4a** and **4b** show AFM images of monolayer graphene with nanopores. These two samples were irradiated by $T = 30^\circ\text{C}/P = 30 \text{ W}$ oxygen-plasma for 1s and 2s, respectively. After counting these nanopores in the AFM images, we

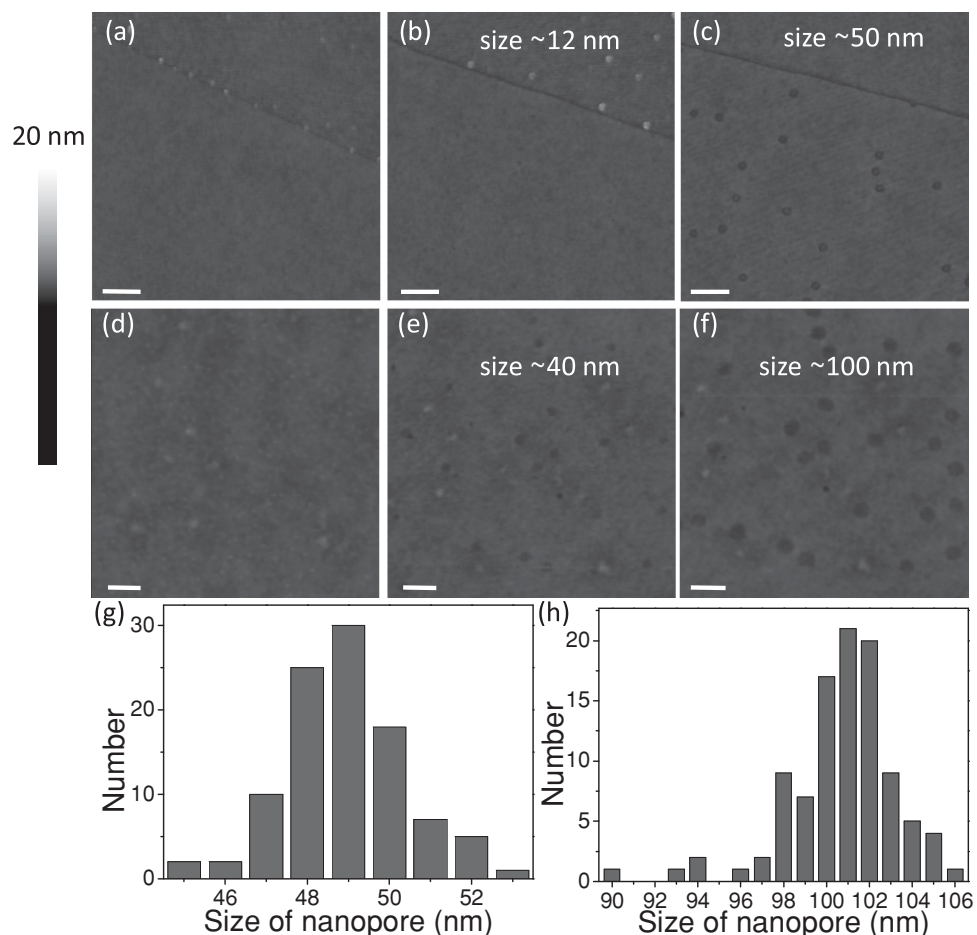


Figure 3. Enlarging defects in graphene into nanopores. (a) AFM image of a typical monolayer graphene after oxygen-plasma irradiation. Corresponding image of the sample after 1 and 4 min hydrogen-plasma etching are shown in (b) and (c), respectively. (d) AFM image of a typical bilayer graphene after oxygen-plasma irradiation. Corresponding image of the sample after 10 and 25 min hydrogen-plasma etching are shown in (e) and (f), respectively. The measured pore sizes in each image are marked. (g)-(h) A size distribution of 100-nanopore in (c) and (f), respectively. Scale bar: 200 nm; color scale bar: 20 nm.

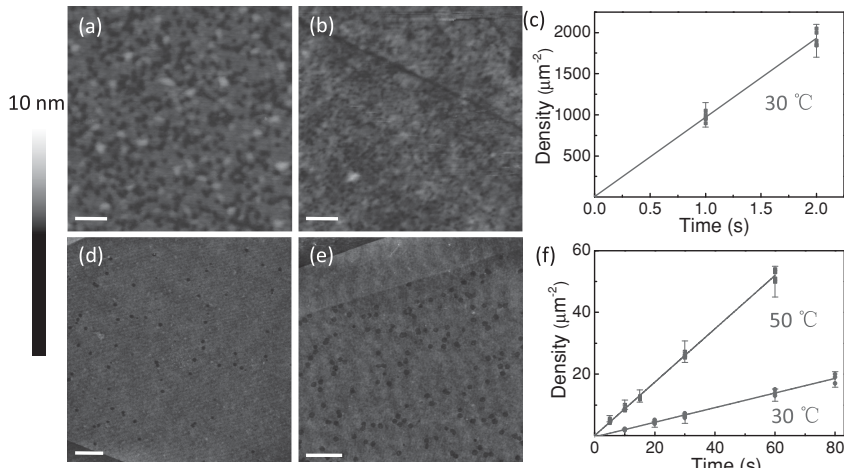


Figure 4. Estimation of defect density by counting the nanopores. (a)-(b) AFM images of enlarged nanopores in monolayer graphene resulted from oxygen-plasma treatment at $T = 30^\circ\text{C}/P = 30\text{W}/t = 1\text{s}$ and $T = 30^\circ\text{C}/P = 30\text{W}/t = 2\text{s}$. (c) Pore density as a function of t for the samples shown in (a-b). (d)-(e) AFM images of enlarged nanopores in bilayer graphene resulted from oxygen-plasma treatment at $T = 30^\circ\text{C}/P = 50\text{W}/t = 20\text{s}$ and $T = 50^\circ\text{C}/P = 50\text{W}/t = 30\text{s}$. (f) Pore density as a function of t for the samples shown in (d-e). The density of detected graphene nanopores increased linearly with t . Scale bar: 100 nm (a, b), 500 nm (d, e); color scale bar: 10 nm.

got the density of $\approx 1 \times 10^3 \mu\text{m}^{-2}$ and $2 \times 10^3 \mu\text{m}^{-2}$ for the samples shown in Figure 4a and 4b, respectively. Figure 4c was the fitting plot of the pore densities with the increase of oxygen etching time, which was rather equal with that deduced by the ratio of $I(D)/I(G)$ from Raman spectra in Figure 2b. Figure 4d ($T = 30^\circ\text{C}/P = 50\text{W}/t = 20\text{s}$) and 4e ($T = 50^\circ\text{C}/P = 50\text{W}/t = 30\text{s}$) show nanopores in bi-layer graphene, and the pore density of bi-layer graphene as a function of oxygen plasma etching time t was shown in Figure 4f. The red (blue) line was the fit of the relationship at 30°C (50°C). The density of detected bi-layer graphene nanopores increased linearly with t . The nanopore density of bi-layer graphene treated by oxygen plasma at 50°C was about four times of that at 30°C . Compared with monolayer graphene, bi-layer graphene was less reactive to oxygen plasma. Moreover, graphene epitaxial growth on hexagonal boron nitride substrate was also applied for the defect and nanopore engineering.^[43] The etching rate of monolayer graphene was much lower than that on SiO_2 .

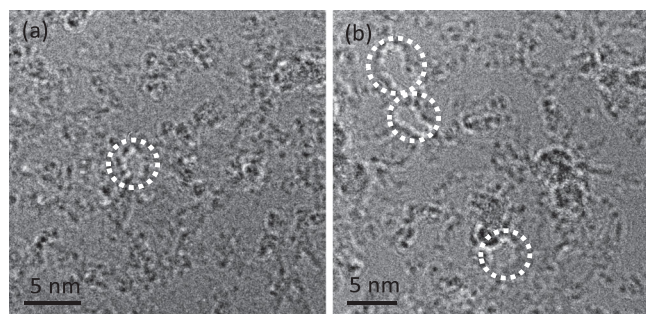


Figure 5. TEM images of nanopores created in monolayer graphene. (a) Image of an ultra-small pore found with a size of $\approx 2\text{ nm}$. (b) Image of three nanopores with sizes $\approx 5\text{ nm}$. 2 s oxygen-plasma followed by 5 s hydrogen-plasma etching and 2 s oxygen-plasma followed by 10 s hydrogen-plasma etching was carried out for the two samples individually.

(shown in Figure S4 in the Supporting Information). It is worth pointing out that the etching rate of bilayer graphene was comparable with that of monolayer sample, which is different from that on SiO_2 . We attribute this to the effect of the substrate. The smoother the substrate, the slower the etching rate is.

2.3. The Smallest Nanopores in Graphene

Nanopores in graphene with different sizes are useful for various applications.^[12,16] Graphene nanopores with size of several angstroms can be used for molecular sieving; while nanopores size of few nanometers can be used for DNA sequencing. For such purpose, we also fabricated nanopores in graphene aiming to achieve ultra-small pore size. Monolayer graphene was transferred on a transmission electron microscope (TEM) grid and then treated by oxygen-plasma at

$T = 30^\circ\text{C}/P = 30\text{ W}$ and subsequent hydrogen-plasma etching. **Figure 5a** and **5b** show two high resolution transmission electron microscope (HRTEM) images for monolayer graphene samples treated by oxygen- and hydrogen-plasma. 2 s oxygen-plasma followed by 5 s hydrogen-plasma etching and 2 s oxygen-plasma followed by 10 s hydrogen-plasma etching was carried out for the two samples individually. The as-resulted nanopores have sizes of $\approx 2\text{ nm}$ (Figure 5a) and $\approx 5\text{ nm}$ (Figure 5b), respectively. The black contamination in the TEM images are PMMA residuals adsorbed during the sample transfer procedure. Such small pore size is comparable with the smallest ones fabricated by focused electron-beam irradiation,^[24] and moreover this approach shows advance in fabrication scalability with a time-efficient manner.

3. Conclusion

We have developed an approach for engineering of defects or nanopores in graphene. Oxygen plasma irradiation was employed to create lattice defects in graphene; and subsequent hydrogen plasma etching was applied to further enlarge these defects into nanopores. We realized a tunable defect density (from a few to $10^3 \mu\text{m}^{-2}$) and pore size ($\approx 2\text{--}100\text{ nm}$) via controlling the plasma treatment conditions. This approach is simple, efficient and controllable, thus providing a scale-up fabrication of defects or nanopores in graphene for various device applications.

Acknowledgements

This work was supported by from the National Basic Research Program of China (973 Program, grant No. 2013CB934500), the

National Science Foundation of China (NSFC, grant Nos. 91223204, 61325021, 11204358, and 11174333), and the Chinese Academy of Sciences.

- [1] Y. W. Son, M. L. Cohen, S. G. Louie, *Nature* **2006**, *444*, 347.
- [2] D. W. Boukhvalov, M. I. Katsnelson, *Nano Lett.* **2008**, *8*, 4373.
- [3] J. Lahiri, Y. Lin, P. Bozkurt, I. I. Oleynik, M. Batzill, *Nat. Nanotechnol.* **2010**, *5*, 326.
- [4] O. V. Yazyev, S. G. Louie, *Nat. Mater.* **2010**, *9*, 806.
- [5] M. M. Ugeda, I. Brihuega, F. Hiebel, P. Mallet, J. Y. Veuillen, J. M. Gomez-Rodriguez, F. Yndurain, *Phys. Rev. B* **2012**, *85*, 121402.
- [6] A. Nourbakhsh, M. Cantoro, T. Vosch, G. Pourtois, F. Clemente, M. H. van der Veen, J. Hofkens, M. M. Heyns, S. De Gendt, B. F. Sels, *Nanotechnology* **2010**, *21*, 435203.
- [7] M. D. Stoller, S. J. Park, Y. W. Zhu, J. H. An, R. S. Ruoff, *Nano Lett.* **2008**, *8*, 3498.
- [8] S. Murali, M. D. Stoller, C. Morales, A. Velamakanni, Y. W. Zhu, R. Ruoff, *ECS Trans.* **2011**, *33*, 99.
- [9] H. M. Jeong, J. W. Lee, W. H. Shin, Y. J. Choi, H. J. Shin, J. K. Kang, J. W. Choi, *Nano Lett.* **2011**, *11*, 2472.
- [10] D. B. Wells, M. Belkin, J. Comer, A. Aksimentiev, *Nano Lett.* **2012**, *12*, 4117.
- [11] C. A. Merchant, K. Healy, M. Wanunu, V. Ray, N. Peterman, J. Bartel, M. D. Fischbein, K. Venta, Z. T. Luo, A. T. C. Johnson, M. Drndic, *Nano Lett.* **2010**, *10*, 2915.
- [12] G. F. Schneider, S. W. Kowalczyk, V. E. Calado, G. Pandraud, H. W. Zandbergen, L. M. K. Vandersypen, C. Dekker, *Nano Lett.* **2010**, *10*, 3163.
- [13] A. Meller, L. Nivon, D. Branton, *Phys. Rev. Lett.* **2001**, *86*, 3435.
- [14] C. Merchant, *Biophys. J.* **2011**, *100*, 521.
- [15] D. Branton, D. W. Deamer, A. Marziali, H. Bayley, S. A. Benner, T. Butler, M. Di Ventra, S. Garaj, A. Hibbs, X. H. Huang, S. B. Jovanovich, P. S. Krstic, S. Lindsay, X. S. S. Ling, C. H. Mastrangelo, A. Meller, J. S. Oliver, Y. V. Pershin, J. M. Ramsey, R. Riehn, G. V. Soni, V. Tabard-Cossa, M. Wanunu, M. Wiggin, J. A. Schloss, *Nat. Biotechnol.* **2008**, *26*, 1146.
- [16] D. E. Jiang, V. R. Cooper, S. Dai, *Nano Lett.* **2009**, *9*, 4019.
- [17] S. Blankenburg, M. Bieri, R. Fasel, K. Mullen, C. A. Pignedoli, D. Passerone, *Small* **2010**, *6*, 2266.
- [18] H. L. Du, J. Y. Li, J. Zhang, G. Su, X. Y. Li, Y. L. Zhao, *J. Phys. Chem. C* **2011**, *115*, 23261.
- [19] J. Schrier, *J. Phys. Chem. Lett.* **2010**, *1*, 2284.
- [20] A. W. Hauser, P. Schwerdtfeger, *J. Phys. Chem. Lett.* **2012**, *3*, 209.
- [21] K. Sint, B. Wang, P. Kral, *J. Am. Chem. Soc.* **2008**, *130*, 16448.
- [22] L. Liu, S. M. Ryu, M. R. Tomasik, E. Stolyarova, N. Jung, M. S. Hybertsen, M. L. Steigerwald, L. E. Brus, G. W. Flynn, *Nano Lett.* **2008**, *8*, 1965.
- [23] G. Lee, B. Lee, J. Kim, K. Cho, *J. Phys. Chem. C* **2009**, *113*, 14225.
- [24] M. D. Fischbein, M. Drndic, *Appl. Phys. Lett.* **2008**, *93*, 113107.
- [25] L. S. Weng, L. Y. Zhang, Y. P. Chen, L. P. Rokhinson, *Appl. Phys. Lett.* **2008**, *93*, 093107.
- [26] Z. Y. Zeng, X. Huang, Z. Y. Yin, H. Li, Y. Chen, H. Li, Q. Zhang, J. Ma, F. Boey, H. Zhang, *Adv. Mater.* **2012**, *24*, 4138.
- [27] B. Ozylmaz, P. Jarillo-Herrero, D. Efetov, P. Kim, *Appl. Phys. Lett.* **2007**, *91*, 192107.
- [28] D. C. Kim, D. Y. Jeon, H. J. Chung, Y. Woo, J. K. Shin, S. Seo, *Nanotechnology* **2009**, *20*, 375703.
- [29] I. Childres, L. A. Jauregui, J. F. Tian, Y. P. Chen, *New J. Phys.* **2011**, *13*, 025008.
- [30] X. C. Yang, S. J. Tang, G. Q. Ding, X. M. Xie, M. H. Jiang, F. Q. Huang, *Nanotechnology* **2012**, *23*, 025704.
- [31] L. Ci, Z. P. Xu, L. L. Wang, W. Gao, F. Ding, K. F. Kelly, B. I. Yakobson, P. M. Ajayan, *Nano Res.* **2008**, *1*, 116.
- [32] C. J. Russo, J. A. Golovchenko, *Proc. Natl. Acad. Sci. USA* **2012**, *109*, 5953.
- [33] L. Liu, D. L. Xie, M. H. Wu, X. X. Yang, Z. Xu, W. L. Wang, X. D. Bai, E. G. Wang, *Carbon* **2012**, *50*, 3039.
- [34] T. Kato, L. Y. Jiao, X. R. Wang, H. L. Wang, X. L. Li, L. Zhang, R. Hatakeyama, H. J. Dai, *Small* **2011**, *7*, 574.
- [35] R. Yang, L. C. Zhang, Y. Wang, Z. W. Shi, D. X. Shi, H. J. Gao, E. G. Wang, G. Y. Zhang, *Adv. Mater.* **2010**, *22*, 4014.
- [36] Z. W. Shi, R. Yang, L. C. Zhang, Y. Wang, D. H. Liu, D. X. Shi, E. G. Wang, G. Y. Zhang, *Adv. Mater.* **2011**, *23*, 3061.
- [37] G. B. Xie, Z. W. Shi, R. Yang, D. H. Liu, W. Yang, M. Cheng, D. M. Wang, D. X. Shi, G. Y. Zhang, *Nano Lett.* **2012**, *12*, 4642.
- [38] S. Wu, R. Yang, D. X. Shi, G. Y. Zhang, *Nanoscale* **2012**, *4*, 2005.
- [39] F. Tuinstra, J. L. Koenig, *J. Chem. Phys.* **1970**, *53*, 1126.
- [40] M. M. Lucchese, F. Stavale, E. H. M. Ferreira, C. Vilani, M. V. O. Moutinho, R. B. Capaz, C. A. Achete, A. Jorio, *Carbon* **2010**, *48*, 1592.
- [41] A. C. Ferrari, J. Robertson, *Phys. Rev. B* **2000**, *61*, 14095.
- [42] A. C. Ferrari, *Solid State Commun.* **2007**, *143*, 47.
- [43] W. Yang, G. R. Chen, Z. W. Shi, C. C. Liu, L. C. Zhang, G. B. Xie, M. Cheng, D. M. Wang, R. Yang, D. X. Shi, K. Watanabe, T. Taniguchi, Y. G. Yao, Y. B. Zhang, G. Y. Zhang, *Nat. Mater.* **2013**, *12*, 792.

Received: November 28, 2013

Revised: February 12, 2014

Published online: March 7, 2014